

University of Groningen

## The cooling phase of Type-I X-ray bursts in 4U 1636–53

Zhang, Guobao; Mendez, Mariano; Altamirano, Diego

*Published in:*  
Monthly Notices of the Royal Astronomical Society

*DOI:*  
[10.1111/j.1365-2966.2011.18271.x](https://doi.org/10.1111/j.1365-2966.2011.18271.x)

**IMPORTANT NOTE:** You are advised to consult the publisher's version (publisher's PDF) if you wish to cite from it. Please check the document version below.

*Document Version*  
Publisher's PDF, also known as Version of record

*Publication date:*  
2011

[Link to publication in University of Groningen/UMCG research database](#)

*Citation for published version (APA):*

Zhang, G., Mendez, M., & Altamirano, D. (2011). The cooling phase of Type-I X-ray bursts in 4U 1636–53. *Monthly Notices of the Royal Astronomical Society*, 413(3), 1913–1921. <https://doi.org/10.1111/j.1365-2966.2011.18271.x>

**Copyright**

Other than for strictly personal use, it is not permitted to download or to forward/distribute the text or part of it without the consent of the author(s) and/or copyright holder(s), unless the work is under an open content license (like Creative Commons).

The publication may also be distributed here under the terms of Article 25fa of the Dutch Copyright Act, indicated by the “Taverne” license. More information can be found on the University of Groningen website: <https://www.rug.nl/library/open-access/self-archiving-pure/taverne-amendment>.

**Take-down policy**

If you believe that this document breaches copyright please contact us providing details, and we will remove access to the work immediately and investigate your claim.

*Downloaded from the University of Groningen/UMCG research database (Pure): <http://www.rug.nl/research/portal>. For technical reasons the number of authors shown on this cover page is limited to 10 maximum.*

# The cooling phase of Type-I X-ray bursts in 4U 1636–53

Guobao Zhang<sup>1\*</sup>, Mariano Méndez<sup>1</sup> and Diego Altamirano<sup>2</sup>

<sup>1</sup>*Kapteyn Astronomical Institute, University of Groningen, P.O. BOX 800, 9700 AV Groningen, The Netherlands*

<sup>2</sup>*Astronomical Institute, “Anton Pannekoek”, University of Amsterdam, Science Park 904, 1098 XH Amsterdam, The Netherlands*

14 October 2010

## ABSTRACT

Time-resolved spectra during the cooling phase of thermonuclear X-ray bursts in low-mass X-ray binaries (LMXBs) can be used to measure the radii and masses of neutron stars. We analyzed  $\sim 300$  bursts of the LMXB 4U 1636–53 using data from the Rossi X-ray Timing Explorer. We divided the bursts in three groups, photospheric radius expansion (PRE), hard non-PRE and soft non-PRE bursts, based on the properties of the bursts and the state of the source at the time of the burst. For the three types of bursts, we found that the average relation between the bolometric flux and the temperature during the cooling phase of the bursts is significantly different from the canonical  $F \propto T^4$  relation that is expected if the apparent emitting area on the surface of the neutron star remains constant as the flux decreases during the decay of the bursts. We also found that a single power law cannot fit the average flux-temperature relation for any of the three types of bursts, and that the flux-temperature relation for the three types of bursts is significantly different. Finally, for the three types of bursts, the temperature distribution at different flux levels during the decay of the bursts is significantly different. From the above we conclude that hard non-PRE bursts ignite in a hydrogen-rich atmosphere, whereas for soft non-PRE and PRE bursts the fuel is helium-rich. We further conclude that the metal abundance in the neutron star atmosphere decreases as the bursts decay, probably because the heavy elements sink faster in the atmosphere than H and He.

**Key words:** stars: neutron — X-rays: binaries — X-rays: bursts — stars: individual: 4U 1636–53

## 1 INTRODUCTION

Thermonuclear, type-I, X-ray bursts are due to unstable burning of H and He on the surface of accreting neutron stars in low-mass X-ray binaries (LMXBs). During these bursts, the observed X-ray intensity first sharply increases, typically by a factor of  $\sim 10$  in about 0.5–5 seconds, and after that it decreases more or less exponentially within 10–100 seconds (e.g., Lewin et al. 1993; Strohmayer & Bildsten 2006; Galloway et al. 2008). The total energy emitted by an X-ray burst is typically  $\sim 10^{39}$  ergs. Some X-ray bursts are strong enough to lift up the outer layers of the star. During these so-called photospheric radius expansion (PRE) bursts (Basinska et al. 1984), the radiation flux that emerges from the stellar surface is limited by the Eddington flux. The neutron-star surface origin is supported by the fact that the inferred emission area during a burst matches the expected surface area of a neutron star, assuming that the thermonuclear flash expands to cover the entire star during

the radius expansion and cooling phases of the burst. The emission area can be estimated from the fitting of the energy spectra during the cooling tails of bursts. There are a number of theoretical and observational arguments that support this assumption (see, e.g. Fryxell & Woosley 1982; Bildsten 1995; Spitkovsky et al. 2002; Strohmayer & Bildsten 2006).

One of the best studied sources of X-ray bursts is the LMXB 4U 1636–53. Also known as V801 Ara, 4U 1636–53 was discovered with OSO-8 (Swank et al. 1976), and was subsequently studied in great detail using observations with SAS-3, Hakucho, Tenma, and EXOSAT (see Lewin et al. 1987, for a review). The orbital period of this binary system is 3.8 hr (van Paradijs et al. 1990), and the spin period of the neutron star is 581 Hz (Strohmayer et al. 1998a,b). Using EXOSAT, Damen et al. (1989) detected 60 bursts from this source between 1983 and 1986; from observations with the Rossi X-ray Timing Explorer (RXTE), 172 bursts were detected up to 2007 June 3 (Galloway et al. 2008), and more than 250 bursts including data taken after that date (Zhang et al. 2009). Most of these X-ray bursts have standard, single-peaked, fast rising and expo-

\* E-mail: zhang@astro.rug.nl

nentially decaying light curves. Some single-peaked bursts show photospheric radius expansion, while a few other bursts from 4U 1636–53 show multi-peaked light curves, although these are not PRE bursts (Maurer & Watts 2008; Bhattacharyya & Strohmayer 2006a; Zhang et al. 2009).

In this paper, we compare the temperature and emission-area distributions in PRE non-PRE and double-peaked bursts during their cooling phase.

## 2 OBSERVATION AND DATA ANALYSIS

We analyzed all data available from the RXTE Proportional Counter Array (PCA) of 4U 1636–53 as of May 2010. The PCA consists of an array of five collimated proportional counter units (PCUs) operating in the 2–60 keV range. We produced 1-s light curves from the Standard1 data (0.125-s time resolution with no energy resolution) and searched for X-ray bursts in the light curves. We used the 16-s time-resolution Standard-2 data to calculate X-ray colours of the source, as described in Zhang et al. (2009). Hard and soft colours are defined as the 9.7 – 16.0/6.0 – 9.7 keV and 3.5 – 6.0/2.0 – 3.5 keV count rate ratios, respectively, and intensity as the 2.0 – 16.0 keV count rate. The colour-colour diagram (CD) of all observations of 4U 1636–53 is shown in Figure 1. The position of the source on the diagram is parameterized by the length of the solid curve  $S_a$  (see, e.g. Méndez et al. 1999). The  $S_a$  length is normalized to the distance between  $S_a = 1$  at the top right vertex, and  $S_a = 2$  at the bottom left vertex of the CD. Similar to the  $S_z$  length in Z sources (Vrtilek et al. 1990),  $S_a$  is considered to be a function of mass accretion rate (Hasinger & van der Klis 1989).

In order to study the bursts in detail, we analyzed the PCA Event data, E\_125us\_64M\_0.1s, in which each individual photon is time tagged at a  $\sim 122 \mu\text{s}$  time resolution in 64 energy channels between 2 – 60 keV. We used all PCUs that were operating at the time of the X-ray burst to produce 0.5-s resolution light curves in the full PCA band. For the time-resolved spectral analysis of the bursts we extracted spectra in 64 channels every 0.5 s from the Event data of all available PCUs. We corrected each spectrum for dead time using the methods supplied by the RXTE team. We generated the instrument response matrix files for each observation, and we fitted the spectra using XSPEC version 12.4.0. Because of the short exposure, in this case the statistical errors dominate, and therefore we did not add any systematic error to the spectra. We restricted the spectral fits to the energy range 3.0 – 20.0 keV. For each burst we extracted the spectrum from the persistent data just before (or after) the burst to use as background in our fits; this approach, used to obtain the net emission of a burst, is well established as a standard procedure in X-ray burst analysis (e.g. Kuulkers et al. 2002). We fitted the time-resolved net burst spectra with a single-temperature blackbody model (bbodyrad in XSPEC), as generally burst spectra are well fitted by a blackbody. During the fitting, we kept the hydrogen column density  $N_H$  fixed at  $0.36 \times 10^{22} \text{cm}^{-2}$  (Pandel et al. 2008), and to calculate the radius of the emitting area in km, we assumed a distance of 5.95 kpc (Fiocchi et al. 2006). The model provides the blackbody colour temperature ( $T_{\text{bb}}$ ) and a normalization proportional to the square of the blackbody radius

( $R_{\text{bb}}$ ) of the burst emission surface, and allows us to estimate the bolometric flux as a function of time.

We note that this procedure fails if the blackbody emission during the burst comes from the same source that produces the blackbody emission seen in the persistent emission, since the difference between two blackbody spectra is not a blackbody (van Paradijs & Lewin 1986). This effect is significant only when the net burst emission is small, and therefore problems may arise only at the start and tail of the burst, when the net burst emission is comparable to the underlying persistent emission (see the discussion in Kuulkers et al. 2002).

To test whether fitting the net spectrum of the bursts affects our results, we proceeded as follows: For a subsample of the bursts we fitted the persistent spectrum just before each burst with a blackbody and a power law. During the burst, we fixed the power-law index and normalization to the value of the persistent emission, and let the blackbody parameters to vary. Using this procedure we found results that are consistent with the ones we found using the standard method therefore, in the rest of the paper, we used the results we obtained using the standard method

We defined the cooling phase for different types of bursts observed in 4U 1636–53 as follows: The cooling phase of non-PRE single-peaked and PRE bursts starts from the moment that the fitted blackbody temperature starts to decrease until the end of the burst, defined as the time when the burst flux is within  $3\sigma$  of the pre-burst persistent emission. For double-peaked bursts we used two different definitions of the cooling phase, one that starts from the moment the blackbody temperature starts to decrease after the first peak of the burst until the end of the burst, and the other one from the moment the blackbody temperature starts to decrease after the second peak of the burst until the end of the burst. We did not consider the triple-peaked burst reported in Zhang et al. (2009)

## 3 RESULT

### 3.1 Temperature distribution during the cooling phase of X-ray bursts

In order to understand the cooling tails of PRE, single-peaked non-PRE, and double-peaked bursts, we fitted the time-resolved spectra with an absorbed blackbody and compared the fitting parameters. From the CD in Figure 1 and hardness-intensity diagram (HID) in Figure 2, we found that all the PRE bursts and double-peaked bursts have a hard colour smaller than 0.85 (see also Munro et al. 2004; Zhang et al. 2009). We therefore divided the bursts in four groups based on their persistent hard colour and their time-resolved spectrum (see Figures 1 and 2): (i) Hard non-PRE bursts; these are single-peaked non-PRE bursts that took place when the persistent hard colour of the source was larger than 0.85. (ii) Soft non-PRE bursts; these are single-peaked non-PRE bursts that took place when the persistent hard colour of the source was smaller than 0.85. (iii), PRE bursts; (iv) Double-peaked bursts.

In Figure 3, we investigate the relation between the bolometric flux and the color temperature during the cooling phase of the bursts using 0.5 s bins (see section 2). In this

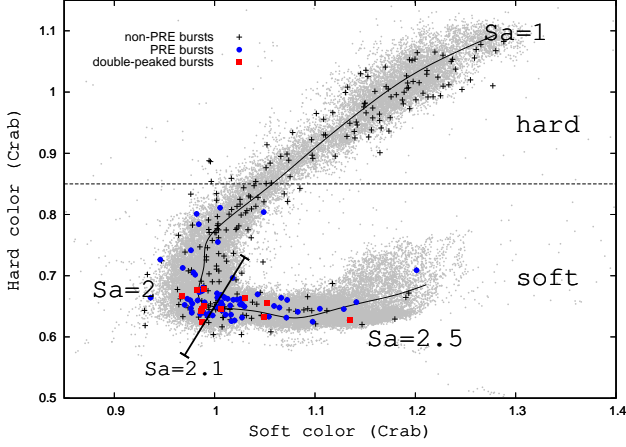


**Figure 1.** Colour-colour diagram of all RXTE observations of 4U 1636-53 up to May 2010. The grey points represent the colours of the source from all available RXTE observations. Each point in this diagram represents 256 s of data. The black crosses represent the colours of the persistent emission of the source at the onset of a single-peaked non-PRE X-ray burst. The filled blue circles indicate the same for PRE burst, and the red squares for double-peaked bursts. The position of the source on the diagram is parameterized by the length of the black solid curve  $S_a$ . The horizontal line divides hard and soft state of the source (see text for details). The diagonal solid bar divides the PRE bursts into two groups ( $S_a > 2.1$  and  $S_a < 2.1$ ; see text for details.)

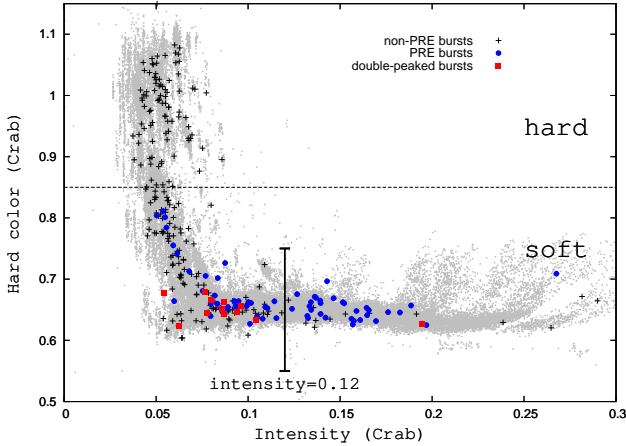


**Figure 2.** Hardness-intensity diagram of all RXTE observations of 4U 1636-53. The symbols are the same as in Figure 1. The PRE bursts are divided into two groups (intensity  $> 0.12$  Crab and intensity  $< 0.12$  Crab) by the vertical solid bar.

so-called flux-temperature (FT) diagram we also show lines of constant inferred radius, calculated from  $F/(\sigma T^4)$ . The top panels (a) and (b) of Figure 3 show the cooling phase of non-PRE bursts and PRE bursts, respectively; the bottom panels (c) and (d) show the cooling phase of double-peaked bursts after the first and second peak, respectively. In order to compare different types of bursts at the same source state, in panel (a) of Figure 3 we only plot the soft non-PRE bursts. At the beginning of the cooling phase (upper left part of the panels), both PRE and soft non-PRE bursts appear to have similar colour temperature. However, at the end of the cooling phase (lower-right part of the panels) the

soft non-PRE bursts appear to have a larger spread of temperatures than the PRE bursts. Comparing the two bottom panels in Figure 3, we notice that there are some points at high flux level but below the 8-km radius red line in panel (c) that are not present in panel (d). These points are the ones between the two peaks in double-peaked bursts. After the second peak, in double-peaked bursts most of the points appear above the red line.

In order to study the distribution of temperatures in the cooling phase of the bursts quantitatively, we divided the data of Figure 3 in four different groups based on flux levels. Panels (a) to (d) in Figure 4 show the distribution of the colour temperature during the cooling phase of hard non-PRE bursts (black), soft non-PRE bursts (red), PRE bursts (green) and double-peaked bursts after the second peak (blue), at different flux levels. In Table 1 we give the average and standard deviation of the distribution of temperatures for each flux level. We find that, as the bolometric flux decreases in the cooling tail, the average temperature of the hard non-PRE bursts becomes significantly higher than that of the soft non-PRE bursts. We also find that, as the flux decreases, the average temperature of soft non-PRE bursts becomes significantly higher than that of PRE bursts and double-peaked bursts. At higher flux levels, the PRE bursts dominate the sample.

We carried out a Kolmogorov-Smirnov (KS) test to assess whether any two distributions are consistent with being the same. The results of the KS tests are shown in Table 2. We find that, except at the highest flux level, it is unlikely that any two sample distributions in Figure 4 come from the same parent population. We note that there are only eleven double-peaked bursts in our sample and therefore the KS-test results are less reliable when we compare other samples to this type of bursts. Since it is apparent that the average temperature of different types of bursts is different (Table 1), we repeated the KS test after we first aligned all distributions such that they all have the same average temperature. The new KS-test results are shown in Table 3. As expected, after aligning the distributions, the probabilities of the KS test increased. But at low flux level, the probability that two samples come from the same parent population remains small. This indicates that in these cases, not only the average, but also the shape of the distributions is different.

### 3.2 Flux-Temperature relation during the cooling phase of X-ray bursts

The evolution of the bolometric flux and the blackbody temperature during the cooling tails of all X-ray bursts in our sample appear to follow a power-law relation. We fitted a power law,  $F_b = \alpha T_{bb}^\gamma$ , to the data for PRE, soft non-PRE and hard non-PRE bursts, separately, where  $F_b$  is the bolometric flux,  $T_{bb}$  is the blackbody colour temperature,  $\alpha$  is the normalization and  $\gamma$  is the power-law index.

For all type of burst, we first selected data with  $\frac{F_b}{\delta F_b} > 2$ , where  $\delta F_b$  is the error of the bolometric flux, and we rebinned the data by a factor 10 (we also tried  $\frac{F_b}{\delta F_b} > 1$  and  $\frac{F_b}{\delta F_b} > 3$ , but the power-law fitting results are consistent with the ones we found using  $\frac{F_b}{\delta F_b} > 2$ ). We then divided the data into three groups: data with  $F_b > 1 \times 10^{-8}$  erg cm $^{-2}$  s $^{-1}$ ,



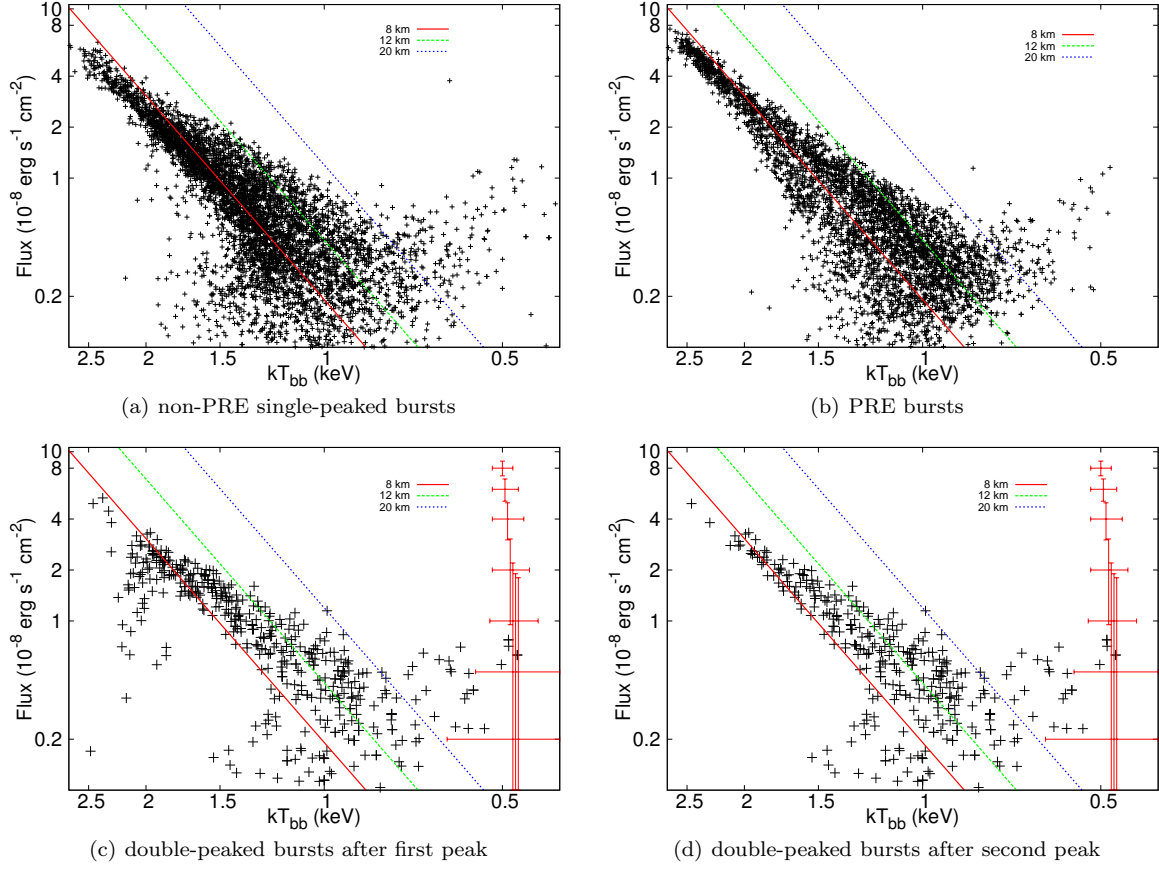


**Figure 3.** Bolometric flux as a function of blackbody colour temperature for different types of bursts in 4U 1636-53 during the cooling phase of the burst. Each point on the plot represent 0.5 seconds. The diagonal lines represent lines of constant inferred radius. Typical 90% confidence level error bars are indicated in the lower panels..

**Table 1.** The average and standard deviation of the temperature distribution for different types of bursts at different flux levels.

| Flux range ( $10^{-8}$ erg $\text{cm}^{-2}$ $\text{s}^{-1}$ ) |  | 0-1.0 | 1.0-2.0 | 2.0-4.0 | 4.0-7.0 |
|---|--|-------|---------|---------|---------|
| hard non-PRE  | $\langle kT_{\text{bb}} \rangle$ (keV) | 1.42  | 1.79    | 2.05    | 2.37    |
|   | $\sigma$ (keV)                         | 0.27  | 0.15    | 0.18    | 0.64    |
| soft non-PRE  | $\langle kT_{\text{bb}} \rangle$ (keV) | 1.21  | 1.61    | 2.01    | 2.42    |
|   | $\sigma$ (keV)                         | 0.23  | 0.21    | 0.20    | 0.38    |
| PRE   | $\langle kT_{\text{bb}} \rangle$ (keV) | 1.09  | 1.58    | 1.98    | 2.36    |
|   | $\sigma$ (keV)                         | 0.23  | 0.20    | 0.19    | 0.19    |
| double-peaked   | $\langle kT_{\text{bb}} \rangle$ (keV) | 0.98  | 1.46    | 1.83    | 2.45    |
|   | $\sigma$ (keV)                         | 0.23  | 0.23    | 0.38    | 1.20    |

$F_b > 2 \times 10^{-8}$  erg  $\text{cm}^{-2}$   $\text{s}^{-1}$ , and all data, and fitted each group separately. The best fitting results are shown in Table 4, and the fits are shown in Figure 5.

A power law fits well the data with flux larger than  $1 \times 10^{-8}$  erg  $\text{cm}^{-2}$   $\text{s}^{-1}$  for all type of bursts, but a power law does not fit all the data (without flux selection) for any of the three types of bursts (see Table 4). We also found that: (i) During the cooling phase, the X-ray bursts of 4U 1636-53 do not follow the expected  $F_b \propto T_{\text{bb}}^4$  relation; (ii) within the same type of bursts, the power-law index changes

significantly as the flux increases; (iii) within the same flux selection, the power-law index of hard non-PRE bursts is significantly higher than that of PRE and soft non-PRE bursts (except at the highest flux level where the fitting errors are large due to the limited data). Given that  $L_b = \alpha T_{\text{bb}}^\gamma$ , this means that for a fixed flux level, hard non-PRE bursts have higher  $T_{\text{bb}}$  than PRE and soft non-PRE bursts as the neutron star cools down or, for a fixed  $T_{\text{bb}}$  during the cooling phase, the apparent emitting area of PRE and soft non-PRE bursts is larger than that of hard non-PRE bursts.

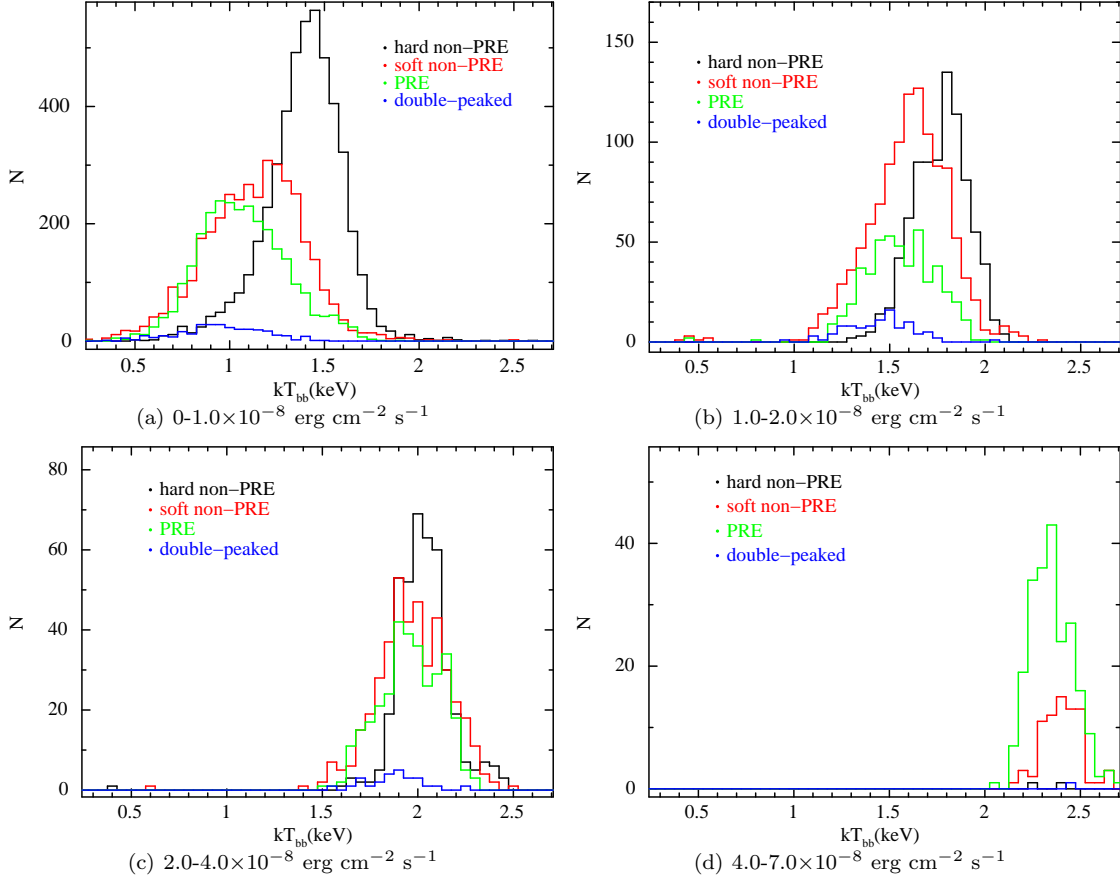


**Figure 4.** The distributions of colour temperatures during the cooling phase for hard non-PRE bursts (blue), soft non-PRE bursts (red), PRE bursts (black) and double-peaked bursts after the second peak (green), respectively. Each panel is for a different flux range, as indicated.

**Table 2.** KS test probabilities for the distributions in Figure 4

| Flux range ( $10^{-8} \text{ erg cm}^{-2} \text{ s}^{-1}$ ) | 0–1.0                | 1.0–2.0               | 2.0–4.0              | 4.0–7.0              |
|---|----------------------|-----------------------|----------------------|----------------------|
| soft non-PRE vs hard non-PRE                                | 0                    | 0                     | $3.0 \times 10^{-8}$ | $7.3 \times 10^{-1}$ |
| soft non-PRE vs PRE   | 0                    | $2.1 \times 10^{-6}$  | $1.5 \times 10^{-1}$ | $0.4 \times 10^{-1}$ |
| hard non-PRE vs PRE   | 0                    | 0                     | $6.2 \times 10^{-9}$ | $9.8 \times 10^{-1}$ |
| soft non-PRE vs double-peaked                               | 0                    | $4.7 \times 10^{-12}$ | $2.9 \times 10^{-2}$ | $6.1 \times 10^{-1}$ |
| PRE vs double-peaked  | $1.1 \times 10^{-7}$ | $3.2 \times 10^{-5}$  | $3.9 \times 10^{-2}$ | $3.5 \times 10^{-1}$ |

### 3.3 Photospheric radius expansion bursts

The PRE bursts concentrate on a narrow range of hard colours in the CD and HID, but they span a large range of soft colours in the CD, and a large range of intensity in the HID. We therefore divided the PRE bursts in two groups according to the position of the source in the CD and HID at the time the bursts started, one group with  $S_a < 2.1$  (low- $S_a$  PRE bursts) and the other with  $S_a > 2.1$  (high- $S_a$  PRE bursts; see the solid bar in Figure 1). We also divided the PRE bursts in two groups according to the intensity of the persistent emission of the source at the time the burst started (see Figure 2): the faint PRE burst, with an inten-

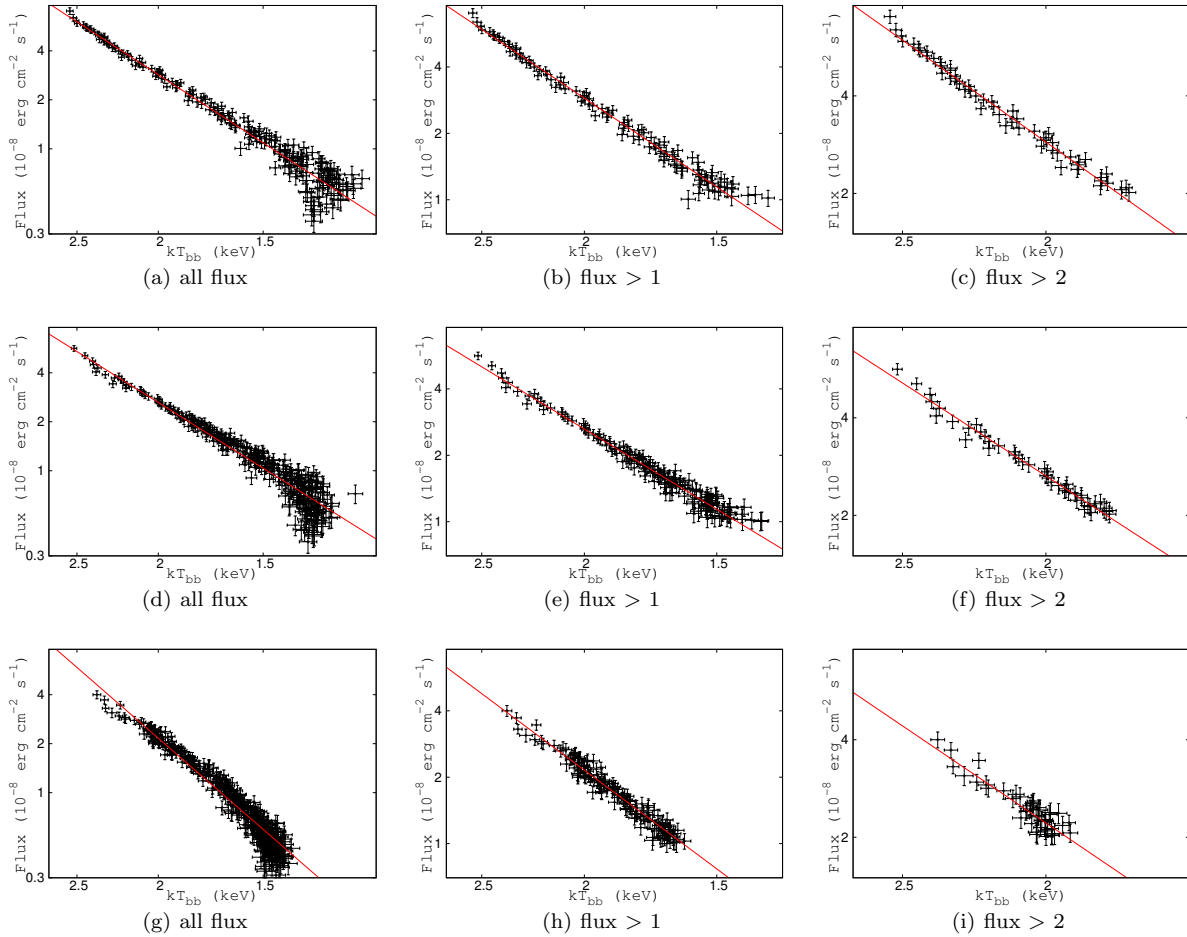
sity lower than 0.12 Crabs, and the bright PRE burst, with an intensity higher than 0.12 Crabs. In panel (a) of Figure 6 we show the distribution of colour temperature during the cooling phase of bright PRE (black) and faint PRE bursts (red), and for low- $S_a$  PRE (red) and high- $S_a$  PRE bursts (black) in panel (b) of Figure 6; in both panel we selected only data with flux less than  $1 \times 10^{-8} \text{ erg cm}^{-2} \text{ s}^{-1}$ . The KS test for these two groups for all flux levels, is shown in Table 5. The KS test still gives small probabilities at the lowest flux level; at other flux levels the samples are consistent with coming from the same parent populations.

**Table 3.** KS test probabilities after we have aligned all the distributions to the same average temperature.

| Flux range( $10^{-8}$ erg cm $^{-2}$ s $^{-1}$ ) | 0–1.0                 | 1.0–2.0              | 2.0–4.0              | 4.0–7.0              |
|--|-----------------------|----------------------|----------------------|----------------------|
| soft non-PRE vs hard non-PRE                     | $2.27 \times 10^{-7}$ | $3.0 \times 10^{-5}$ | $1.1 \times 10^{-2}$ | $9.3 \times 10^{-1}$ |
| soft non-PRE vs PRE                              | $4.6 \times 10^{-5}$  | $1.1 \times 10^{-2}$ | $1.8 \times 10^{-1}$ | $8.4 \times 10^{-1}$ |
| hard non-PRE vs PRE                              | $5.8 \times 10^{-11}$ | $1.6 \times 10^{-2}$ | $1.9 \times 10^{-3}$ | $9.5 \times 10^{-1}$ |
| soft non-PRE vs double-peaked                    | $7.8 \times 10^{-1}$  | $5.9 \times 10^{-1}$ | $1.3 \times 10^{-2}$ | $7.9 \times 10^{-1}$ |
| PRE vs double-peaked                             | $1.8 \times 10^{-2}$  | $7.8 \times 10^{-1}$ | $4.5 \times 10^{-2}$ | $8.3 \times 10^{-1}$ |

**Table 4.** Power-law fit for different types of bursts in the flux-temperature diagram. In the table,  $\alpha$  and  $\gamma$  are the normalization and the index of the best-fitting power law.

| Flux range<br>$10^{-8}$ erg cm $^{-2}$ s $^{-1}$ | all               |                 |                | > 1.0           |                 |                | > 2.0           |                 |                |
|--|-------------------|-----------------|----------------|-----------------|-----------------|----------------|-----------------|-----------------|----------------|
|  | $\alpha$          | $\gamma$        | $\chi^2/d.o.f$ | $\alpha$        | $\gamma$        | $\chi^2/d.o.f$ | $\alpha$        | $\gamma$        | $\chi^2/d.o.f$ |
| PRE  | $0.28 \pm 0.01$   | $3.35 \pm 0.03$ | 420/182        | $0.31 \pm 0.01$ | $3.22 \pm 0.06$ | 120/103        | $0.30 \pm 0.03$ | $3.24 \pm 0.11$ | 42/55          |
| soft non-PRE                                     | $0.28 \pm 0.01$   | $3.23 \pm 0.04$ | 627/256        | $0.35 \pm 0.02$ | $2.91 \pm 0.06$ | 117/147        | $0.34 \pm 0.03$ | $2.96 \pm 0.13$ | 26/44          |
| hard non-PRE                                     | $0.097 \pm 0.004$ | $4.48 \pm 0.06$ | 719/321        | $0.18 \pm 0.01$ | $3.58 \pm 0.12$ | 139/133        | $0.26 \pm 0.06$ | $3.09 \pm 0.31$ | 49/44          |

**Figure 5.** The flux-temperature diagram of PRE (top panels), soft non-PRE (middle panels) and hard non-PRE bursts (bottom panels). From left to right the panels show, respectively, all data, data where the flux was larger than  $1 \times 10^{-8}$  erg cm $^{-2}$  s $^{-1}$ , and data where the flux was larger than  $2 \times 10^{-8}$  erg cm $^{-2}$  s $^{-1}$ . The best-fitting power law for each selection is shown with the red lines.

**Table 5.** KS test probabilities for low  $S_a$  ( $< 2.1$ ) and high  $S_a$  ( $> 2.1$ ) PRE bursts, and bright ( $I > 0.12$  Crab) and faint ( $I < 0.12$  Crab) PRE bursts.

| Flux range ( $10^{-8}$ erg cm $^{-2}$ s $^{-1}$ ) | 0–1.0                 | 1.0–2.0              | 2.0–4.0              | 4.0–7.0              |
|---|-----------------------|----------------------|----------------------|----------------------|
| low $S_a$ vs high $S_a$                           | $7.6 \times 10^{-14}$ | $5.0 \times 10^{-2}$ | $1.3 \times 10^{-2}$ | $3.6 \times 10^{-1}$ |
| bright vs faint                                   | $9.1 \times 10^{-15}$ | $3.6 \times 10^{-1}$ | $4.8 \times 10^{-1}$ | $1.3 \times 10^{-2}$ |

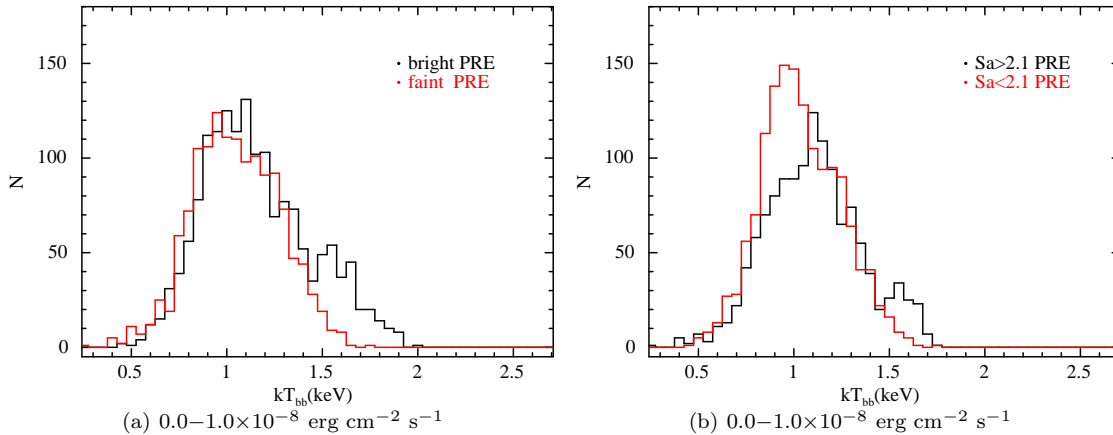


**Figure 6.** The temperature distribution during the cooling phase of PRE bursts with Flux  $< 1 \times 10^{-8}$  erg cm $^{-2}$  s $^{-1}$ . Panel (a) shows PRE bursts with persistent intensity  $> 0.12$  Crab (black) and  $< 0.12$  Crab (red); panel (b) shows the PRE bursts with the  $S_a$  value  $> 2.1$  (black) and  $< 2.1$  (red).

## 4 DISCUSSION

During their cooling phase, the X-ray bursts in 4U 1636–53 do not follow the bolometric flux-temperature relation  $F_b \propto T_{bb}^4$ , which would be expected if the apparent emitting area on the neutron star remained constant during this phase. The relation between bolometric flux and temperature is significantly different between photospheric (PRE) and non-photospheric (non-PRE) bursts, as well as between non-PRE bursts that happen when the source is in the hard state (hard non-PRE bursts) and the soft state (soft non-PRE bursts). We also found that the temperature distribution at different flux levels during the cooling phase is significantly different between PRE, hard non-PRE and soft non-PRE bursts. This is consistent with the fact that different types of bursts have different power-law indices in the flux-temperature diagram.

This result (see also Gottwald et al. 1986; Bhattacharyya et al. 2010; Suleimanov et al. 2010) is at variance with the findings of Güver et al. (2010), who studied three PRE bursts in another source, 4U 1820–30, and found that these PRE bursts follow the  $F_b \propto T_{bb}^4$  relation quite well. Güver et al. (2010), however, did not consider two other PRE bursts in this source because the cooling phase of these two bursts showed a complex behaviour, in which the emitting neutron-star area appeared not to be constant. Here we studied 65 PRE bursts and 223 non-PRE bursts (out of which 94 and 129 were, respectively, hard non-PRE and soft non-PRE bursts), and we did not discard any burst in our sample. While some of the individual bursts in 4U 1636–53 could lay close to

the  $F_b \propto T_{bb}^4$  relation (see Fig. 3), several others deviate significantly from that relation, and on average the relation is significantly different from  $F_b \propto T_{bb}^4$  for any type of burst in our sample. The discrepancy between our results and those of Güver et al. (2010) could be due to differences between the two sources: 4U 1820–30 is an ultracompact binary, with an orbital period of 685s, in which the neutron star accretes He from the companion (Stella et al. 1987; Cumming 2003), whereas 4U 1636–53 has a longer orbital period (3.8 hours; see §1), and the accreted material is mostly hydrogen. It is also possible that the results of Güver et al. (2010) are biased by the small number of bursts they used, three PRE bursts in their case compared to 65 in our case, or by the fact that they ignored two of the PRE bursts in 4U 1820–30 for their analysis.

Time-resolved spectra in the cooling phase of thermonuclear X-ray bursts can be used to measure the radii and masses of neutron stars. The net spectra of the thermonuclear X-ray bursts are usually well described by a blackbody spectrum (Strohmayer & Bildsten 2006; Galloway et al. 2008), which allows us to obtain  $R_{bb}$ ,  $T_{bb}$ , the blackbody radius and colour temperature, respectively, from which we can calculate the bolometric flux of the neutron star. The departure from the  $F_b \propto T_{bb}^4$  relation in the cooling phase of all types of bursts in 4U 1636–53 means that the blackbody radius,  $R_{bb}$ , is not constant during the cooling phase of the bursts. This could be due to either changes in the emitting area of the neutron star during this phase, or to changes in the colour-correction factor, which accounts for hardening of the spectrum arising from electron scattering in the neutron-star atmosphere (London et al. 1986;

Madej et al. 2004) :  $f_c = T_{bb}/T_{eff} = \sqrt{R_\infty/R_{bb}}$ , where  $R_\infty$  is the neutron-star radius observed at infinity.

If  $f_c$  remains constant throughout the cooling phase of all X-ray bursts, the differences of  $R_{bb}$  should be due to the changes of the emission area on the neutron-star surface. From Figure 5 and Table 4, it is apparent that the emission area in hard non-PRE bursts is smaller than in PRE bursts and soft non-PRE bursts, and that at the end of the cooling phase, the emitting area decreases faster in hard non-PRE bursts than in the other types of bursts. Gottwald et al. (1986) also found that in EXO 0748-676 the average  $R_{bb}$  in the cooling phase increases as the persistent flux increases (see also Bildsten 1995). If for hard non-PRE bursts only a fraction of the surface of the neutron star is emitting during the cooling phase, and the size of the emitting area decreases as the burst decays, one would expect to see burst oscillations in the cooling tail of hard non-PRE bursts. However, most bursts with oscillations in 4U 1636-53 occur when the source is in the soft state (Muno et al. 2004).

Alternatively, if  $R_\infty$  should remain constant throughout the cooling phase of all the bursts, variations in  $R_{bb}$  can only be due to changes of  $f_c$ . We can write the colour-correction factor as:

$$f_c = \sqrt{\frac{R_\infty}{d\sqrt{\frac{F}{\sigma T_{bb}^4}}}} = \sqrt{\frac{R(1+z)}{d\sqrt{\frac{F}{\sigma T_{bb}^4}}}}, \quad (1)$$

where  $d$  is the distance to the source,  $R$  is the neutron-star radius,  $z$  is the gravitational redshift, and  $\sigma$  is the Stefan-Boltzmann constant. In Figure 7 we plot  $f_c$  as a function of the neutron-star luminosity in Eddington units. For this plot we assumed  $R = 9$  km,  $(1+z) = 1.35$ ,  $d = 6.0$  Kpc, and we used equation (1) and the same data ( $T_{bb}$  and  $R_{bb}$ ) as in section 3.2. To calculate the fluxes in Eddington units,  $F_b/F_{Edd} = L_b/L_{Edd}$ , for PRE and soft non-PRE bursts we used the average peak flux of PRE bursts as the Eddington flux,  $F_{Edd}$ . Assuming that PRE and soft non-PRE bursts are He bursts, and hard non-PRE bursts are H bursts, for the hard non-PRE bursts we took 59% of the Eddington flux that we used in PRE bursts (assuming a hydrogen mass fraction,  $X = 0.7$ ).

Figure 7 shows that, as the luminosity increases, the colour-correction factor of PRE and soft non-PRE bursts first decreases, then increases, and finally remains more or less constant. For hard non-PRE bursts the colour-correction factor first decreases, and then remains more or less constant as the luminosity increases. At the same luminosity level,  $f_c$  in PRE and soft non-PRE bursts is smaller than in hard non-PRE bursts, while  $f_c$  is consistent with being the same in PRE and soft non-PRE bursts. The data in Figure 7 agree qualitatively with the predictions of the model of Suleimanov et al. (2010) (see their Figure 2), if we assume that during the cooling phase of hard non-PRE bursts the neutron-star atmosphere is H rich, whereas for PRE and soft non-PRE bursts the atmosphere is He rich. At high luminosity levels, the data show that  $f_c$  stays constant, and does not increase as quickly as predicted by the model. We speculate that during the early phases of the cooling phase of all bursts, there is an enhanced abundance of heavy elements in the neutron-star atmosphere that were produced during the thermonuclear flash, and this effect is

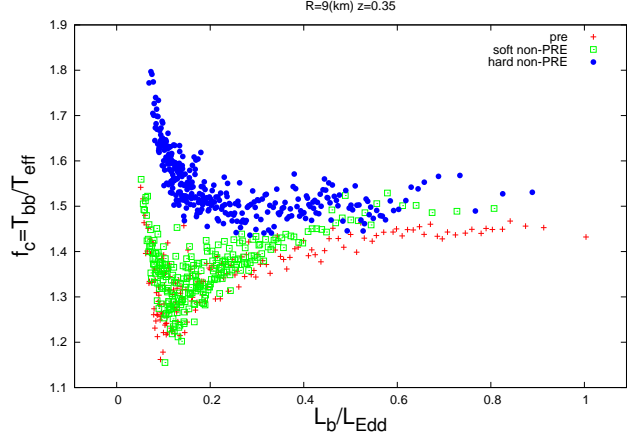


**Figure 7.** Colour-correction factor as a function of luminosity in Eddington units. The different colour points correspond to different types of bursts, as indicated in the plot.

stronger in the PRE and soft non-PRE bursts where dredge up of ashes is more effective (Weinberg et al. 2005); as the neutron-star cools down, the heavy elements settle down faster than H and He, and therefore the heavy-element abundance in the neutron-star atmosphere decreases as the burst decays. This is reported by the models of Suleimanov et al. (2010), in which  $f_c$  decreases as the high-element abundance in the neutron-star atmosphere increases. (The same is true for the model of Güver et al. 2010) It is then possible that the difference at high luminosity between the data and the models of Suleimanov et al. (2010) is due to changes of the chemical composition of the neutron-star atmosphere during the early cooling phase of the bursts.

We also found a significant difference in the distribution of the blackbody temperature during the decay of X-ray bursts in 4U 1636-53 in different types of bursts at different flux levels (see also in Zand et al. 2009; Bhattacharyya et al. 2010). At low flux level, the average  $T_{bb}$  is higher in hard non-PRE bursts than in PRE and soft non-PRE bursts (Figure 4; see also van der Klis et al. 1990). In our sample we have  $\sim 130$  soft non-PRE bursts and  $\sim 90$  hard non-PRE bursts, but in panel (a) of Figure 4, non-PRE bursts have more data points than soft non-PRE bursts. (Remember that each point in that Figure represents a measurement every 0.5 s in the cooling phase of the bursts.) This means that hard non-PRE bursts have longer decay times than PRE and soft non-PRE bursts. The difference of  $T_{bb}$  and burst decay time can also be explained by different chemical composition of the fuel layer (Galloway et al. 2008): If PRE and soft non-PRE bursts ignite in a He-rich environment, most of the fuel is burnt in a very short timescale, and therefore these bursts show fast cooling at the decay phase. The hard non-PRE bursts ignite in a H-rich environment. Hydrogen burning proceeds more slowly, because it is limited by the  $\beta$ -decay moderated by the weak force. During the cooling of hard non-PRE bursts, the Hydrogen left in the atmosphere keeps burning. Also, since the hard non-PRE bursts ignite in a H-rich environment, they have larger  $f_c$  than the PRE and soft non-PRE bursts that ignite in a He-rich environment (Madej et al. 2004; Suleimanov et al. 2010; Güver et al. 2010), therefore

the hard non-PRE bursts show higher average  $T_{\text{bb}}$  than the PRE and soft non-PRE bursts.

We note that the differences in the distribution of  $T_{\text{bb}}$  are more significant at low flux levels. These differences can also be due in part to differences in the underlying emission of the neutron star due to continued accretion during the burst. Van Paradijs & Lewin (1986) argued that the net burst spectrum is not a blackbody, and at the end of the burst the  $T_{\text{bb}}$  of the net burst spectrum is directly related to the neutron-star surface temperature just before the burst. Therefore, differences in the average  $T_{\text{bb}}$  may reflect differences in the neutron-star surface temperature, depending on the state of the source at the time the burst starts. However, there are significant differences in the distribution of  $T_{\text{bb}}$  at low flux levels between PRE and soft non-PRE bursts, whereas both types of bursts occur when 4U 1636–53 is in the soft state, and therefore the persistent spectrum before the bursts should be similar. Also, both types of bursts should ignite in a layer with similar chemical composition, which makes it difficult to explain the differences by differences in the pre-burst persistent emission,  $f_c$  or emission areas.

## 5 CONCLUSIONS

We studied the cooling phase of type-I X-ray bursts in the LMXB 4U 1636–53 using all available RXTE data. We divided the bursts in three groups according to their properties and the spectral state of the source at the time the burst started: Photospheric radius expansion (PRE), hard and soft non-PRE bursts, respectively. (Soft non-PRE and PRE bursts occurred in the soft state of the source.) We found that, during the cooling phase of the bursts:

- For all types of bursts, the average bolometric-flux vs. temperature relation,  $F_b - T_{\text{bb}}$ , is significantly different than the  $F_b \propto T_{\text{bb}}^4$  relation that would be expected if the apparent emitting area on the neutron star remained constant during the decay of the bursts.
- For all types of bursts, the average  $F_b - T_{\text{bb}}$  relation cannot be described by single power law over the whole flux range.
- The average  $F_b - T_{\text{bb}}$  relation is significantly different for PRE, hard non-PRE and soft non-PRE bursts.
- In line with the previous conclusions, the temperature distribution at different flux levels is significantly different for PRE, hard non-PRE and soft non-PRE bursts.

These results imply that either the emitting area on the neutron-star surface or, most likely, the colour-correction factor changes during the cooling phase of X-ray bursts.

We calculated the colour-correction factor separately for the three types of bursts. Compared to the models of Suleimanov et al. (2010), the dependence of the colour-correction factor with luminosity (in Eddington units) is consistent with a scenario in which the main source of fuel in hard non-PRE bursts is hydrogen, whereas for soft non-PRE and PRE bursts the main source of fuel is helium.

Based on the dependence of the colour-correction factor with luminosity at high luminosity, we suggest that at the beginning of the cooling phase of the bursts there is an enhanced metal abundance in the neutron star atmosphere,

and that the relative metal abundance decreases as the burst flux decreases.

## ACKNOWLEDGMENTS

This research has made use of data obtained from the High Energy Astrophysics Science Archive Research Center (HEASARC), provided by NASA’s Goddard Space Flight Center. We thank Jean in’t Zand, Andrew Cumming, Juri Poutanen, Tod Strohmayer, Duncan Galloway and Valery Suleimanov for useful discussions. GZ acknowledges useful discussions with the participants of the Lorentz Center workshop “X-ray bursts and burst oscillations”.

## REFERENCES

- Bhattacharyya S., Strohmayer T. E. 2006a, ApJ, 636, L121  
 Bhattacharyya, S., Miller, M. C., & Galloway, D. K. 2010, MNRAS, 401, 2  
 Basinska, E. M., Lewin, W. H. G., Sztajno, M., Cominsky, L. R., & Marshall, F. J. 1984, ApJ, 281, 337  
 Bildsten, L. 1995, ApJ, 438, 852.  
 Bildsten L., 2000, In: S. S. Holt & W. W. Zhang (ed.) American Institute of Physics Conference Series, vol. 522 of American Institute of Physics Conference Series, 359-369  
 Cumming, A. 2003, ApJ, 595, 1077  
 Damen, E., Jansen, F., Penninx, W., Oosterbroek, T., van Paradijs, J., & Lewin, H. G. 1989, MNRAS, 237, 523  
 Fiocchi, M., Bazzano, A., Ubertini, P., & Jean, P. 2006, ApJ, 651, 416  
 Fryxell, B. A., & Woosley, S. E. 1982, ApJ, 261, 332.  
 Galloway D. K., Muno M. P., Hartman J. M., Savov P., Psaltis D., Chakrabarty D. 2008, ApJS, 179, 360  
 Gottwald, M., Haberl, F., Parmar, A. N., & White, N. E. 1986, ApJ, 308, 213  
 Güver, T., Wroblewski, P., Camarota, L., & Özel, F. 2010b, ApJ, 719, 1807  
 Hasinger, G., & van der Klis, M. 1989, A&A, 225, 79  
 in ’t Zand, J. J. M., Keek, L., Cumming, A., Heger, A., Homan, J., & Méndez, M. 2009, A&A, 497, 469  
 Kuulkers, E., Homan, J., van der Klis, M., Lewin, W. H. G., & Méndez, M. 2002, A&A, 382, 947  
 Lewin, W. H. G., Penninx, W., van Paradijs, J., et al. 1987, ApJ, 319, 893  
 Lewin, W. H. G., van Paradijs, J., & Taam, R. E. 1993, Space Sci. Rev., 62, 223  
 London,  
 Madej, J., Joss, P. C., & Różańska, A. 2004, ApJ, 602, 904  
 Maurer, I., & Watts, A. L. 2008, MNRAS, 383, 387  
 Méndez M., van der Klis M., Ford E. C., Wijnands R., van Paradijs J., 1999, ApJ, 511, L49  
 Muno, M. P., Galloway, D. K., & Chakrabarty, D. 2004, ApJ, 608, 930  
 Pandel, D., Kaaret, P., & Corbel, S. 2008, ApJ, 688, 1288  
 Spitkovsky, A., Levin, Y., & Ushomirsky, G. 2002, ApJ, 566, 1018  
 Stella, L., White, N. E., & Friedhorsky, W. 1987, ApJ, 312, L17

- Strohmayer, T. E., Zhang, W., Swank, J. H., & Lapidus, I. 1998a, *ApJ*, 503, L147
- Strohmayer, T. E., Zhang, W., Swank, J. H., White, N. E., & Lapidus, I. 1998b, *ApJ*, 498, L135
- Strohmayer, T. E., & Bildsten, L. 2006, in *Compact Stellar X-Ray Sources*, ed. W. H. G. Lewin & M. van der Klis (Cambridge: Cambridge Univ. Press).
- Suleimanov, V., Poutanen, J., Revnivtsev, M., & Werner, K. 2010, arXiv:1004.4871
- Swank, J. H., Becker, R. H., Pravdo, S. H., Saba, J. R., & Serlemitsos, P. J. 1976a, *IAU Circ.*, 3000
- van der Klis M., Hasinger G., Damen E., Penninx W., van Paradijs J., Lewin W. H. G. 1990, *ApJ*, 360, L19
- van Paradijs J., Lewin W. H. G. 1986, *A&A*, 157, L10
- van Paradijs, J., et al. 1990, *A&A*, 234, 181
- Vrtilek, S. D., Raymond, J. C., Garcia, M. R., Verbunt, F., Hasinger, G., & Kurster, M. 1990, *A&A*, 235, 162
- Weinberg, N. N., Bildsten, L., & Schatz, H. 2005, *ApJ*, 639, 1018
- Zhang, W., Lapidus, I., Swank, J. H., White, N. E., & Titarchuk, L. 1997, *IAU Circ.* 6541
- Zhang, G. B.; Méndez, M.; Altamirano, D.; Belloni, T. M.; Homan, J.